Lithuanian Journal of Physics
Vol. **65**, No. 2, pp. 107–123 (2025)
ISSN 1648-8504 eISSN 2424-3647
DOI: https://doi.org/10.3952/physics.2025.65.2.3

RADIOGRAPHY AND RADIOTHERAPY OF THE SIMULATED HUMAN TISSUE ENVIRONMENT WITH HIGH-ENERGY PROTONS: A THEORETICAL STUDY

N. Niknam [a], M. Eshghi [b], S.N. Hosseini Motlagh [a], and Z. Parang [a]

[a] *Department of Physics, Shiraz Branch, Islamic Azad University, Shiraz, Iran*
[b] *Department of Physics, Imam Hossein University, Tehran, Iran*
Email: eshgi54@gmail.com, m.eshghi@semnan.ac.ir

Received 17 January 2025; revised 2 July 2025; accepted 21 July 2025

In this research, the diagnostic imaging and therapy of the environment of selected human tissues by the produced protons from fusion reactions have been simulated by using the Geant4 tool. As a result, the stopping power and range of protons with different energies in these tissues have been obtained. As an example, Bragg peaks caused by protons with energies of 60 to 150 MeV have been shown in breast tissue. Further, the penetration depth of protons, proton flux, and the secondary particle flux of neutrons and gamma with energies of 20 to 70 MeV (in the therapeutic energy range) have been investigated in the breast tissue. Finally, a comparison of the residual dose in breast tissue without a tumour and with a tumour at 60 MeV energy has been done. Therefore, with such simulations, calculations, and creative approaches, effective measures can be taken in the fields of proton imaging and proton therapy because proton radiography is a method that can be used to extract the maximum required information from different human tissues. Also, tumours located in different human tissues can be targeted and destroyed by using different energies of protons.

Keywords: Monte Carlo simulation, proton imaging, penetration depth, stopping power, range

1. Introduction

In the rapid ignition approach, the fuel is first compressed to extremely high densities and then rapidly heated using lasers or high-energy beams to achieve the necessary conditions for fusion reactions. One of the most critical reactions in this process is the fusion of deuterium (a heavy hydrogen isotope) with helium-3, which produces helium-4 and high-energy protons while releasing approximately 18.3 MeV of energy, as represented by the following reaction [1–5]:

$$D + {}^{3}He \rightarrow {}^{4}He\ (3.6\ MeV) + p\ (14.7\ MeV). \quad (1)$$

This method offers significant advantages, including the reduced harmful radiation, easier system maintenance and control, and decreased radioactive waste. However, alongside the primary reaction, some secondary reactions may occur, potentially producing materials such as tritium or high-energy neutrons. To address the issue of high-energy neutrons, researchers have proposed converting tritium back into helium-3 for reuse in the fuel cycle.

A valuable by-product of this process is the high-energy protons, which have wide-ranging applications in medicine, particularly in targeted cancer therapy and advanced medical imaging techniques. Compared to other nuclear energy production methods, this technology offers the superior safety as it generates fewer neutrons, reduces the impact on equipment, and is more suitable for medical devices like cyclotrons. The high-energy protons produced can even be utilized in manufacturing specialized radiopharmaceuticals.

For these reasons, the scientific community has shown a particular interest in developing this technology, with extensive ongoing research in the field. The ultimate objectives extend beyond a clean and efficient energy production to include creating innovative medical capabilities and industrial applications. These advancements could bring about fundamental transformations in both the energy and medical sectors. Therefore, many authors have done

various research works using the protons produced from the fast combustion reaction, Eq. (1). For example, see Refs. [6–8].

In terms of proton application, all human materials and tissues are medically important and can be investigated because the use of protons allows a better dose conformation (due to the localised Bragg peak at the end of the proton range in the tissue) [9]. Second, proton velocity is inversely proportional to the energy transferred to the traversed tissue, which is reduced during their path as electromagnetic interactions occur with tissue atoms [10]. Third, protons provide a very precise and localised dose deposition in depth. However, protons lose 20–30% of beam energy while passing through matter, and nuclear reactions generate radioactive descendants and secondary nuclei, which are usually β+ emitters that decay rapidly [11]. Also, the dose deposited by secondary protons and charged particles is limited to the area surrounding the beam's path from the entrance surface to the target volume, whereas secondary neutrons scatter further, leading to the whole body neutron dose exposure [12, 13] and the activation of surrounding materials [14]. Further, protons are particles that are commonly used in various medical applications such as imaging and proton therapy to treat cancer.

In proton imaging, several interaction processes with matter must be considered. The most important interaction of charged particles with the environment in terms of energy loss is nuclear interactions and multiple Coulomb scattering. In fact, radiography is one of the important methods of non-destructive testing that is used to identify internal defects, both metallic and non-metallic ones. In the radiography test, the amount of different absorption of nuclear radiation when passing through the medium of the material is used. The part of the beam that is absorbed when passing through the medium of the material depends on the thickness, density, atomic number of the material, the type and energy of the passing rays. If there is a defect, heterogeneity, density change or thickness change in the tissue or material, the amount of absorbed radiation will be different at different points. Therefore, radiography is a method that is used in order to extract the maximum required information from inside a material environment. Using this information, you can get a two-dimensional or three-dimensional image of the desired environment. Information extraction is done by processing raw primary data or predictions obtained from the boundaries of the desired object [15, 16]. In the field of proton radiography, many researches have been done [17–22]. Further, Sheng et al. (2024) have used amide proton transfer-weighted (APTw) imaging to detect the biochemical status of human tissue lesions [23]. Chang et al. (2023) have used diffusion-weighted imaging (DWI) and amide proton transfer-weighted (APTw) imaging to predict preoperative pathologic grades of bladder cancer [24]. Also, Berthold et al. (2021) have presented the first systematic validation of CT-based proton range prediction in prostate cancer treatments using prompt gamma imaging (PGI) [25]. Shiraishi et al. (2024) have assessed the delivered doses to the rectal walls using PET/CT after proton beam therapy [26]. Also, in view of the importance for identifying and differentiating tissues in diagnostic imaging as well as for estimating the accurate dose in radiotherapy and particle-beam therapy, Özpolat et al. (2020) have introduced the Phy-X/ZeXTRa software for the fast and accurate calculation in a wide energy range for both photon and charged particle (electrons, protons, alpha particles and C ions) interactions [27].

In proton therapy, the range and stopping power of protons in different tissues are very important to optimize treatment planning and ensure effective treatment results. The stopping power of protons is a measure of their energy loss per unit path length in the tissue. It determines the rate at which protons store their energy along their path. The stopping power of protons is influenced by factors such as the density and composition of the tissue, the atomic number of the atoms that make up the tissue, and the energy of the protons themselves. Bethe was the first person to use the stopping power case from the study of quantum mechanics. The Bethe formula or the Bethe–Bloch formula describes the average energy loss per distance travelled by fast charged particles (protons, alpha particles and atomic ions) passing through matter (or alternatively the stopping power of matter) [28]. In this theory, the target is assumed to be a charged particle. Charged particles moving in the material interact with the atomic electrons in the material. This interaction excites or ionizes the atoms, causing the moving particle to lose energy. In tissues, protons interact with atomic nuclei, mainly through Coulomb interactions. These interactions lead to energy loss through ionization and excitation processes. With the penetration of

protons into the tissues, their energy gradually decreases and, as a result, there is a range that depends on the initial energy of the proton and the properties of the tissue. Using the different energy of the protons can target and destroy tumours located in different human tissues. Also, by using different energies of the protons, different physical quantities can be calculated in the field of proton dosimetry and radiotherapy.

In this area, Mehmet Büyükyıldız has investigated various human organs, and tissues have been studied in terms of the effective atomic numbers (Z_{eff}) and electron densities (N_e) in the continuous kinetic energy region for different types of heavy ions [29]. Also, Büyükyıldız and Kurudirek have investigated the radiological properties of healthy, carcinoma and equivalent breast tissues for photon and charged particle interactions [30].

Therefore, in this research, we investigate the creation of the image formed by protons passing the models of different human tissues using the Geant4 simulation tool. We convert the extracted data results into the images of desired textures using the Origin software. In the following, we examine the depth of penetration of protons and the amount of proton flux passing through the desired tissue, the stopping power and range of protons in these tissues.

2. Materials and work methods

2.1. Geant4 simulation tool

The Monte Carlo simulation method is a powerful tool for radiation physicists, and several general-purpose software packages are commonly used in a myriad of different areas of radiation physics. Geant4 simulation is one of these tools. This tool is written in the C++ programming language and based on the transport of different types of particles in the environment.

Geant4 has extensive libraries that include the cross section (probability of interaction) of different particles and in different environments. Among the prominent features of this code is its free and high ability to design geometry, particle interaction physics and radiation source. This tool provides interfaces for its users to interact with their program and save their results.

Currently, the heavy projects of the CERN research centre in Europe and many other projects, including fundamental particle physics, dosimetry design and treatment, microdosimetry in the intracellular space, protection of spaceships, design and optimization of radiation therapy devices, and muon tomography, are performed using this tool [31, 32].

2.2. Materials used in proton radiography

As we mentioned in the Introduction, in reaction of tdeuteron with helium-3 nuclei, deuterons can combine with the target fuel helium-3 and produce heavy charged particles such as alpha and protons (Fig. 1).

Considering that the energy of the produced protons is low, it is necessary to increase their energy so that it is suitable for the purposes of radiography and radiotherapy.

To increase the energy of protons from 14.7 MeV to higher energies, one may use a cyclotron, which is a type of a circular accelerator that

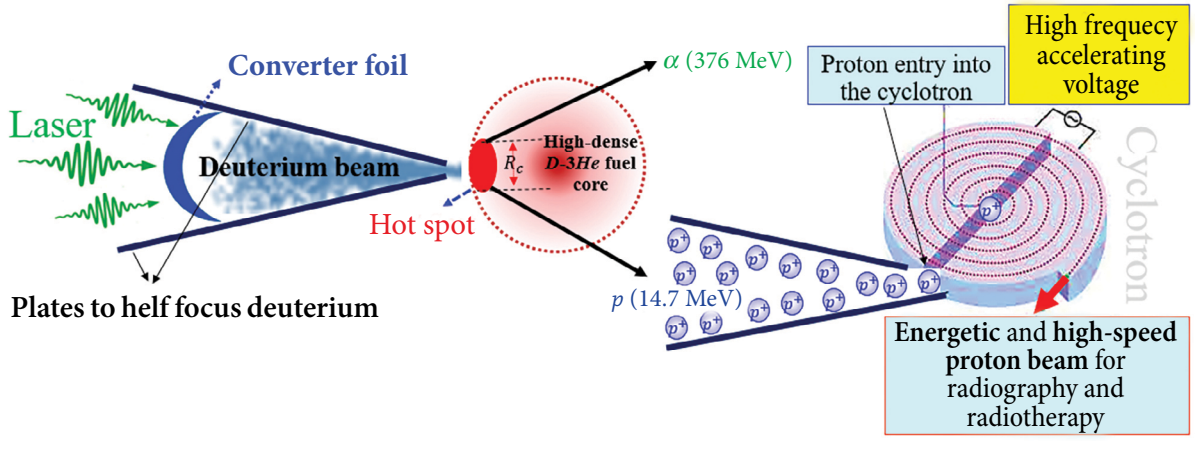

Fig. 1. Schematic of the high-speed proton beam production process for radiography and radiotherapy.

uses a combination of electric and magnetic fields to accelerate protons. Cyclotrons are capable of reaching high energies and are commonly used in medical facilities for proton therapy. In this research, proton energies of 20 to 150 MeV will be used.

Also, we are ready to simulate our selected human tissues (the selection of tissues is random and optional) to create a proton image. For this, we visualize the geometric shapes equivalent to human tissue, for example, lung, brain, testicle, ovary, breast, blood, skin, heart, water and soft tissue, with different dimensions and geometries according to Fig. 2.

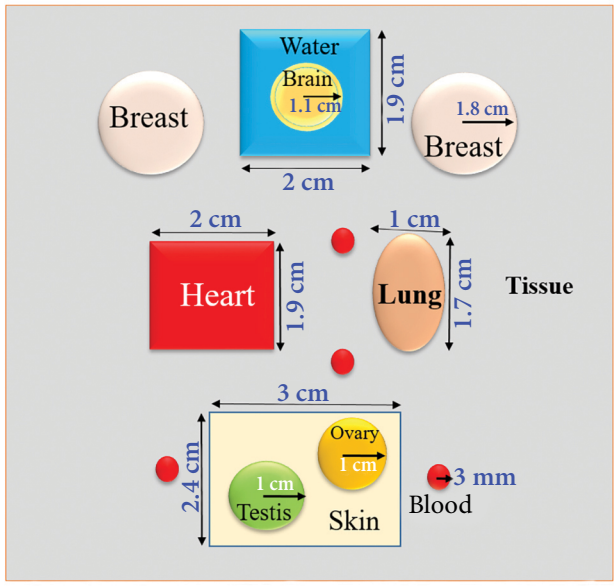

Fig. 2. Schematic of the various body tissues (breast, brain, heart, lung, skin, testis, ovary and blood) is shown inside an imaginary cube.

Only one noteworthy point is the choice of water, which is equivalent to human tissues. In fact, in the calculations of stopping power and proton range or similar calculations performed in relation to human tissue, the use of water is common for the following reasons:

- *Structural similarity*: water has a simple structure and consists of two hydrogen atoms and one oxygen atom. This simple structure and the similarity of water to the structure of living cells and tissues, for example, watery tissues such as skin, muscles and blood vessels, make water to be considered as a representative model for these tissues.
- *Physical properties*: water has unique physical properties that make it the best material for simulating and investigating the electronic and mechanical properties of living materials. For example, water exhibits electrical conductive properties and electrostatic interactions much better than other materials.
- *Easy access*: water is easily accessible and available. This allows researchers to use water as a very common test material in biophysical and medical physics studies in their experiments and calculations.

However, using water as a model for proton stopping power and range calculations or human tissue simulation does not necessarily mean that water is completely similar to these systems, but is used due to its structural simplicity, physical properties, and an easy access.

Anyway, we model the radiation of protons with different energies on human tissues (we do not consider the sizes to be real for simplicity) using the Geant4 simulation tool.

We point out that the proton imaging system can be performing in three ways, according to the type of interaction with matter, firstly, via the method of weakening charged particles, secondly, via the method of nuclear scattering, and thirdly, via the method of tracking particles with energy loss [33]. Each of the mentioned methods is selected and used depending on the purpose of imaging.

Here, using the proton attenuation method, the image of body tissues is extracted in the form of proton flux output from different tissues. With this method, the spatial resolution and the density resolution are effective in the quality of the images taken from the considered materials. The characteristics of all the different textures of Fig. 2 are presented in Table 1 [34].

2.3. Stopping power and range of protons

The two parameters of stopping power and proton range are the most important parameters studied in radiography and proton therapy. In fact, understanding the range and stopping power of protons in tissue is critical to optimizing treatment planning and ensuring effective treatment outcomes. Theoretically, in Bethe's theory, the projectile heavy particle can be assumed to be structureless, while the target nucleus is infinitely heavy. For the energy range of charged particles from 0.04 to 200 MeV, the mass stopping power equation can be expressed as follows [35–38]:

Table 1. Chemical compounds of the human tissue [34].

Human tissue	Density, g/cm^3	Composition (element: fraction) by atom fraction									
		H	C	N	O	Na	P	S	Cl	K	Fe
Ovary	1.05	0.105	0.093	0.024	0.768	0.002	0.002	0.002	0.002	0.002	–
Blood	1.06	0.102	0.11	0.033	0.745	0.001	0.001	0.002	0.003	0.002	0.001
Testis	1.04	0.106	0.099	0.02	0.766	0.002	0.001	0.002	0.002	0.002	–
Water	1	0.112	–	–	0.888	–	–	–	–	–	–
Skin	1.09	0.10	0.204	0.042	0.645	0.002	0.001	0.002	0.003	0.001	–
Lung	1.05	0.103	0.105	0.031	0.749	0.002	0.002	0.003	0.003	0.002	–
Breast	0.99	0.106	0.332	0.003	0.527	0.001	0.001	0.002	0.001	–	–
Brain	1.04	0.107	0.145	0.022	0.712	0.002	0.004	0.002	0.003	0.003	–
Heart	1.06	0.103	0.121	0.032	0.734	0.001	0.001	0.002	0.003	0.002	0.001
Soft tissue	1.03	0.105	0.256	0.027	0.602	0.002	0.001	0.002	0.003	0.001	–

$$-\frac{\mathrm{d}E}{\rho \mathrm{d}x} = \frac{5.08\times10^{-31} Z^2 n}{\beta^2 \rho}[F(\beta) - \ln I]\cdot \tag{2}$$

Here $\beta = v/c$ (v is the speed of proton and c is the speed of light), Z is the atomic number, I is the average excitation energy, and $F(\beta)$ is obtained as

$$F(\beta) = \ln\frac{1.02\times10^6 \beta^2}{1-\beta^2} - \beta^2, \tag{3}$$

and n in Eq. (2) is calculated using the equation

$$n = N_A \rho \langle Z/A \rangle, \tag{4}$$

where N_A is Avogadro's number, ρ is the density of the material, and Z/A is the ratio of the atomic number to the mass number of the material.

Also, all incident protons with a certain energy have a certain range in the target material. By definition, the range of protons refers to the distance that they can travel in a given material before losing most of their energy. The range R for an incident proton in the CSDA method is given as [37–40]

$$R = \int_{E_0}^{E_f} \frac{\mathrm{d}E}{\mathrm{MS}(E)}, \tag{5}$$

where E_0 is the initial energy of the charged particle impacting on the material, E_f is the final energy of the charged particle impacting on the material, and MS(E) is the mass stopping power.

With this introduction, when a charged particle (such as a proton) passes through a material, it causes the atoms of the material to ionize.

This causes the radiation dose to be deposited in the target material during the passage of the particle.

By reducing the energy of the charged particle during its passage through the material, the cross-sectional area of its interaction with the material increases and increases the dose of radiation received by this part of the material. In this way, a peak is created at the end of the charged particle dose distribution curves according to the penetration depth from the surface of the material. This curve is called 'Bragg curve' and the peak in the curve is called 'Bragg peak' [41]. The highest dose distribution of the charged particle in this area occurs when passing through the investigated material. Depending on the depth of the treated cancer tissue from the body surface, the energy of the impinging charged particle is adjusted so that the Bragg peak of the dose distribution curve is located at the depth where the tumour is located. In this way, the maximum energy transfer of the charged particle is transferred to the cancerous tissue and causes tumour damage. In fact, the unique feature of protons is that it allows for more localized dose deposition within the tumour and minimizes damage to surrounding healthy tissues.

Here, we have simulated a breast phantom using the Geant4 tool. We assume that the main breast is a deep structure, the small tumour is located at some distance from the outer surface of the breast tissue. Therefore, in this case, by irradiating single-energy protons (Pencil Beam) to the breast tissue, we calculate and check the stopping power and range of protons with energies of 60 to 150 MeV. The most energy released in the tumour belongs to

the Bragg peak formation area and the most damage will be done to the tumour in this energy.

3. Results and discussions

In this section, we present the simulation results and discuss each of them below.

3.1. Proton imaging of tissue

The created images are the final product against which a system is judged. Here, given the possible differences in goals and requirements that an imaging system may have, we limit our discussion to a simple, idealized proton imaging system. Here, we show the reproduced proton images of the examples of phantoms containing selected human tissues with the specific dimensions and geometries of Fig. 3.

These figures are produced by simulated radiation of protons with energies of 104 to 118 MeV upon the different tissues of the images. The reason for choosing these energies is that there is a practical barrier to many current facility setups: they typically cannot access proton energies above 230 MeV (33 cm range), which is necessary for imaging many parts of the body. With the same assumption, we reduced the energy of the protons by half so that we can have a low-energy proton image of the tissues. Due to the fact that protons in the tissue environment do not follow direct paths due to their different interactions with their atoms, they create an image blur.

Accordingly, it is clearly visible that the more the energy increases in proton radiation upon different tissues, the better the image quality. In fact, the acceptability of any design depends on the imaging quality (spatial separation and noise) and the imaging location of the environment. Also, the closer the proton source is to the surface of the patient's tissue, the higher the spatial resolution and quality of the images. Regarding the imaging quality, it is important to place the imaging receiver as close as possible to the target tissue to reduce the blurring effects caused by a proton scattering in it.

3.2. Stopping power and range of protons in the tissue

Proton transport imaging requires protons to pass through the patient to reach the detector. Whereas proton therapy requires the stopping of protons in the vicinity of the tumour because the most important feature of high-energy proton beams is the discharge of energy in the form of a Bragg curve and the possibility of creating a broadened Bragg peak, in order to completely cover the tumour. In fact, in proton therapy, when protons reach body tissues, they can release their energy at a certain depth according to the location of the tumour. Therefore, by directing the proton beams towards the cancer and stopping them inside the tumour, cancer is destroyed while doing little damage to the nearby healthy cells because the tissues behind and in front of the tumour are exposed to very little radiation.

With these interpretations, considering the importance of calculating the amount of residual energy in the target tissue in terms of dosimetry and also investigating the energy loss of the projectile in terms of protection, it is particularly important to check and calculate the stopping power and range of different ions in different targets. By accurately calculating the stopping power of ions, their range can be determined with a good accuracy. Here, we calculate the stopping power and range of protons in terms of proton energy for different tissues and show the results in Figs. 4 and 5.

As seen in Fig. 4, the stopping power values for different tissues such as lung, testis, breast, brain, blood, skin, liver, cancerous tumour and water increase exponentially and reach a maximum value with the increase in the energy of radiation protons. In the following, these values begin to decrease exponentially.

According to Fig. 5, the range values of most of the mentioned tissues are almost close to each other and similarly and exponentially, they increase with the increase of radiation proton energy.

3.3. Bragg peak and penetration depth of protons in breast tissue

In particular, the breast tissue was irradiated with different proton energies and the Bragg curve at each energy was drawn for this tissue in Fig. 6.

Here, a view of the Bragg peak at different proton energies is shown, with each specific colour representing the results for a specific proton energy because the Bragg peaks originate from a single-energy proton beam. Considering that the formation

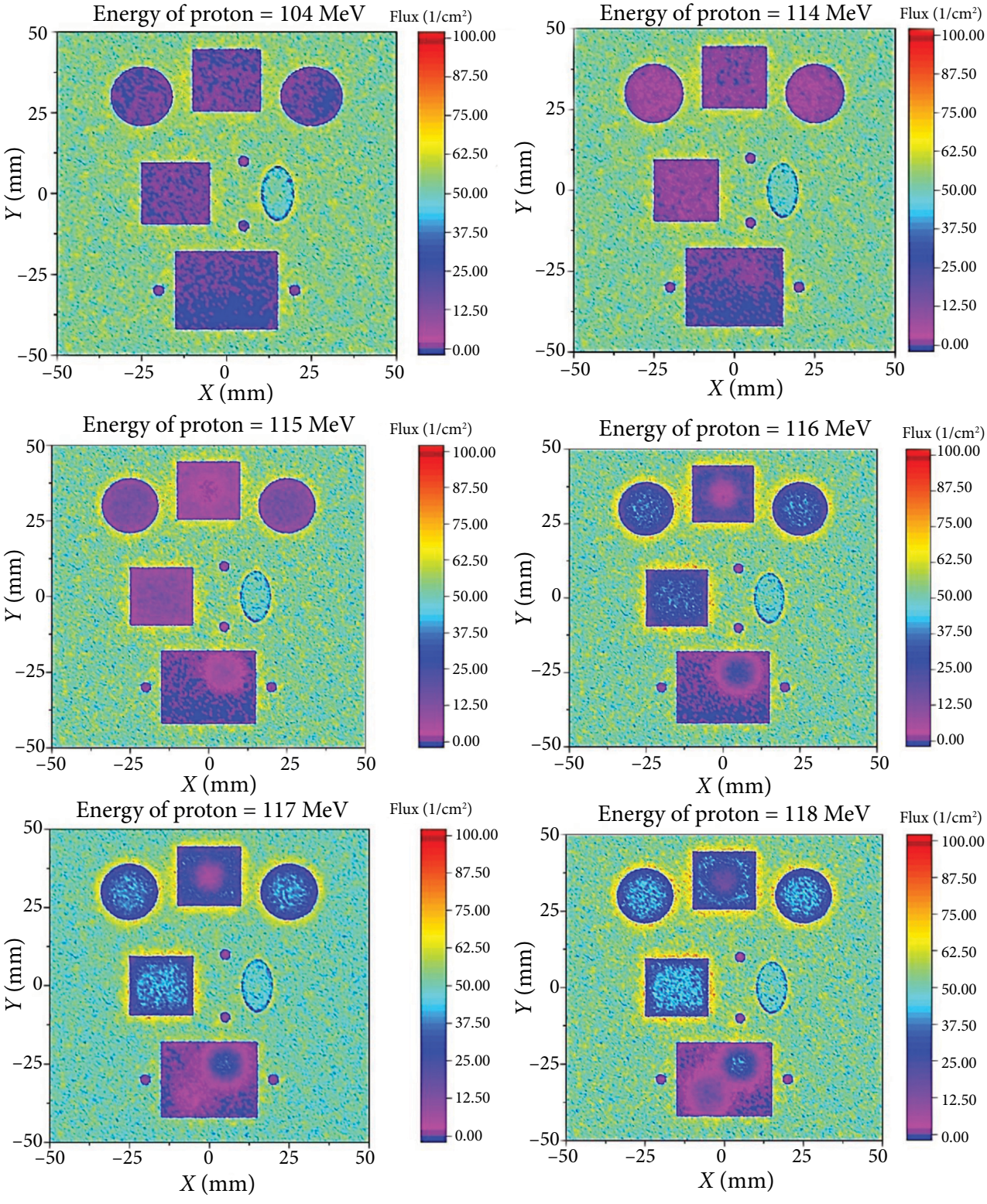

Fig. 3. Schematic images of different tissues (breast, brain, heart, lung, skin, testis, ovary and blood) with protons with different energies of 104, 114, 115, 116, 117 and 118 MeV.

of Bragg peaks is caused by a single-energy proton beam, it is necessary to create an extended Bragg peak to cover the tumour created in the breast tissue. In this figure, it is clear that with the increase of incident proton energy (60, 70, 80, 90, 100, 110, 120, 130, 140 and 150 MeV), the number of inelastic collisions with material nuclei increases, and this causes the height of the Bragg peak to decrease with its depth increasing from 3 to 16 cm. The reason for increasing the energy of the protons up to

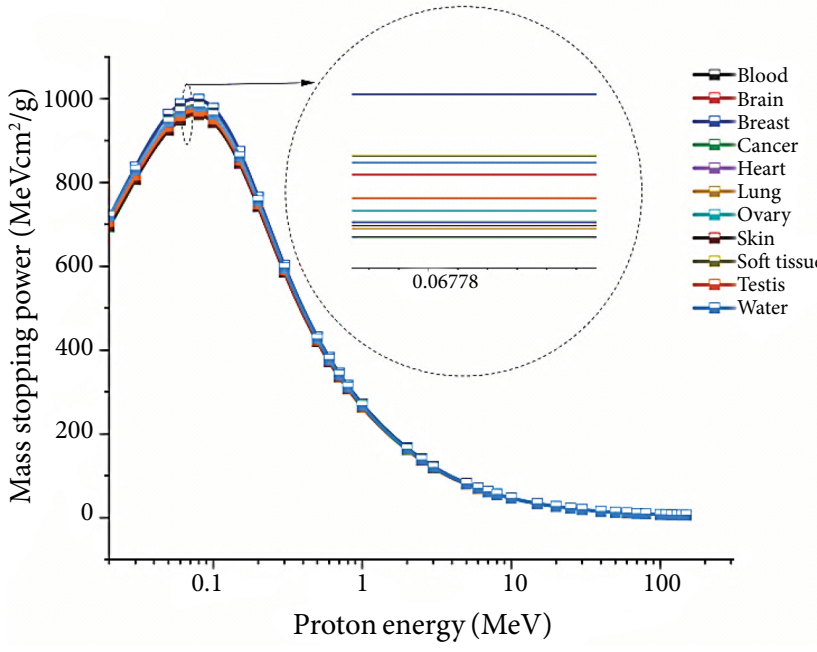

Fig. 4. Schematic of the configuration of the mass stopping power of protons in terms of energy for different human phantom tissues.

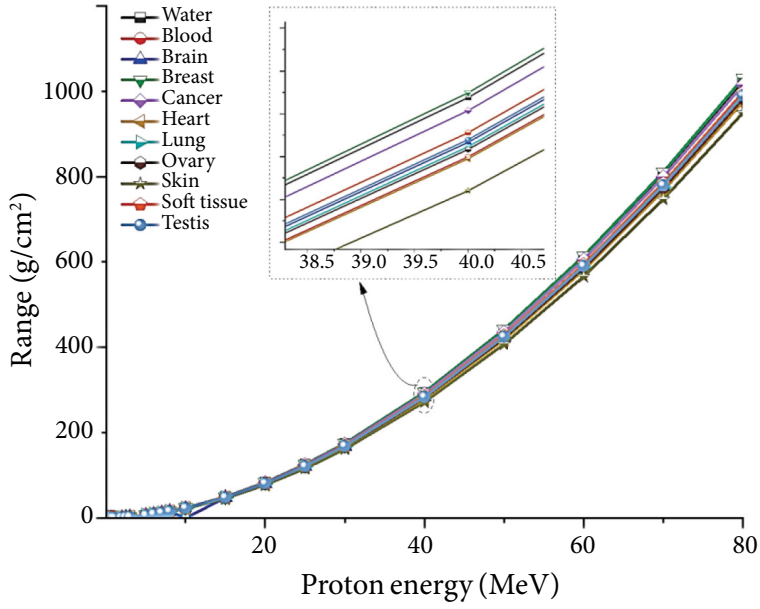

Fig. 5. Schematic of the configuration of the range of protons in terms of energy for different tissues of the human phantom.

150 MeV was that the size of the breast tissue may be larger than usual. Also, in this figure, it is clear that firstly, the expected dependence of penetration depth and Bragg peak size is on the incident beam energy, and a lesser dependence on the incident beam radius is also evident. Secondly, with these single proton energies considered, the Bragg peaks are located inside the breast tissue, and it is observed that the particle penetration power increases with the increase of proton energy. Thirdly, the energy of incident protons has been depleted faster in the breast tissue. More precisely, the sharper the slope of the graph, the faster the proton energy is discharged in the breast tissue. Fourth, the average residual energy of a proton, from the moment of contact to stopping in the depth of the breast tissue as the Bragg peak, at the energy of 60 MeV is more than 70 and 80 MeV.

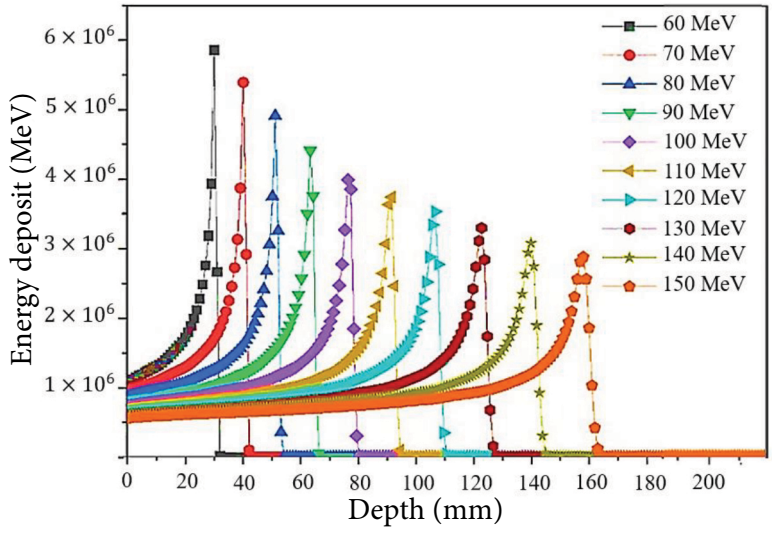

Fig. 6. Schematic of the Bragg peak formed in the breast at different proton energies. Each specific colour shows the results of each proton energy in MeV.

For the proper treatment plan, it is necessary to discharge most energy in the tumour site, and the effect of proton energy in the breast tissue can be fully investigated. Therefore, the flux of protons with energies of 20, 30, 40, 50, 60 and 70 MeV has been evaluated in terms of penetration depth in the breast tissue in Fig. 7. Here, the proton flux is highest at the beginning of the path and then gradually decreases as the protons pass inside the breast tissue due to the gradual decrease in proton energy. Therefore, the possibility of interaction of these protons with the nuclei of the environment increases, and suddenly they disappear at the end of the path.

In the interaction of low-energy protons with the nuclei of the environment and with the reduction of proton energy due to scattering from these nuclei, a group of secondary particles (neutron, proton, electron, deuteron, helium, triton and alpha particles) are produced in addition to photons (gamma rays and X-rays). This situation is clearly evident, and the flux of secondary neutrons (i.e. the result of the interaction of particles with the environment) and the flux of secondary photons (caused by

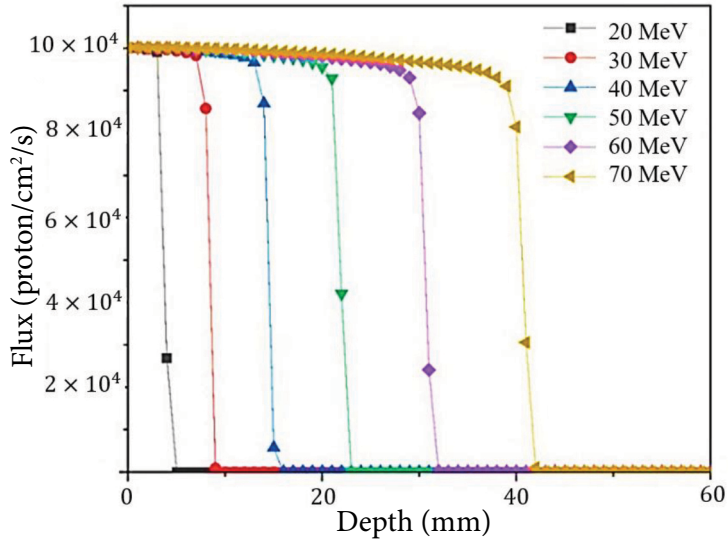

Fig. 7. Proton flux (proton/cm^2/s) according to the penetration depth (mm) in the breast.

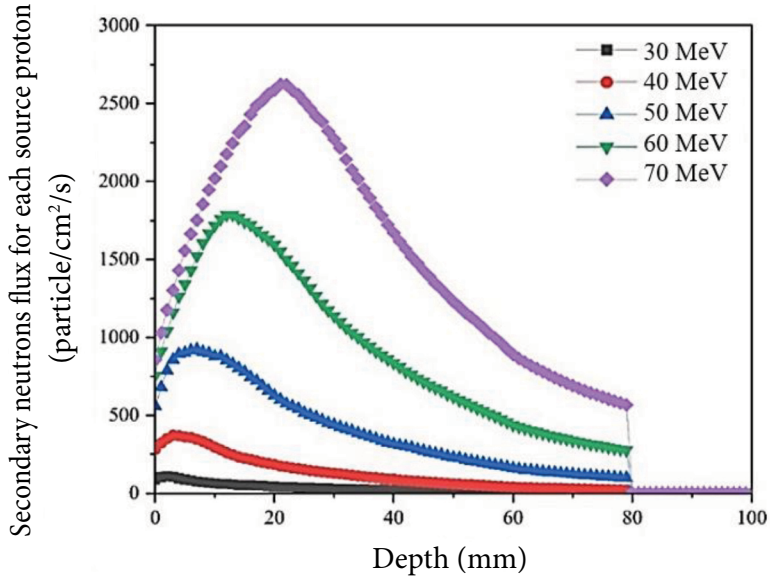

Fig. 8. Flux of secondary neutron particles for each proton source with different energies according to the penetration depth in the breast tissue.

the interaction of particles with the environment) in the breast tissue as a function of the depth inside the tissue for each proton source is shown in Figs. 8 and 9, respectively. Figure 8 shows the secondary neutron particle flux for each proton source with different energies based on the penetration depth in the breast tissue. The flux of secondary neutrons is low at the beginning of the path of this figure, but as the depth increases, the secondary neutrons increase and form a peak to return and decrease again. Therefore, when a beam of high-energy protons reaches the breast tissue, the cross-section of neutron production reaction is low. When the proton beam travels a distance in the breast tissue, its speed decreases and the cross-section of neutron production increases gradually. With the greater proton energy,

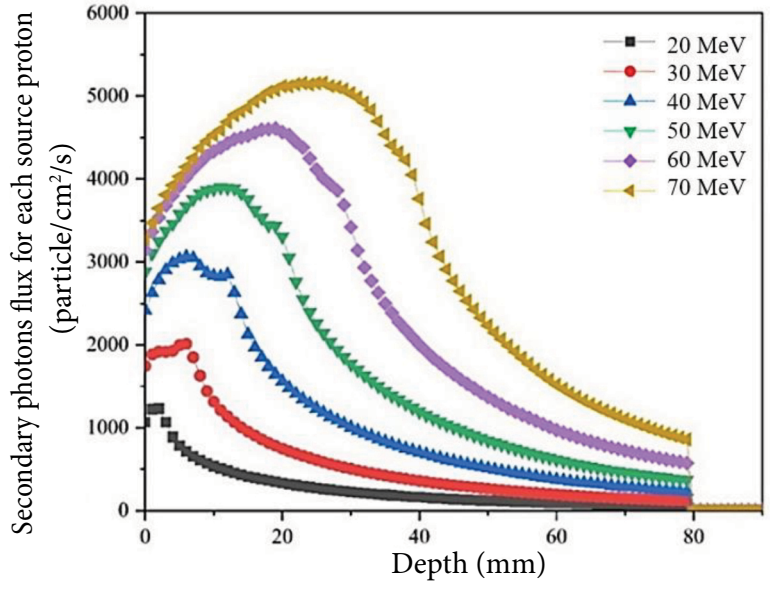

Fig. 9. Flux of secondary photon particles for each proton source with different energies according to the penetration depth in the breast tissue.

the cross-section of neutron production and consequently the neutron flux are greater, and at certain distance a peak of the total neutron product resulting from the interaction of the proton with the nuclei of the tissue environment is formed; then, the flux of secondary particles decreases exponentially according to the penetration depth in the tissue.

Figure 9 shows the secondary photon particle flux for each proton source with different energies based on the penetration depth in the breast tissue. In this figure, most of these photons originate from the interaction of secondary neutrons with the nuclei of the environment, in addition to the interaction of protons and other particles. Therefore, the speed of photon generation dramatically reaches the speed of secondary neutron interaction. In fact, the flux of secondary photons, like the flux of secondary neutrons, is low at the beginning of the path in Fig. 9, but with the increase in depth, the secondary photons increase and form a peak to return and reduce the flux of photons again.

We see the two-dimensional contour images of the energy discharged in the breast tissue for single-energy radiation proton energies of 20, 30, 40, 50, 60 and 70 MeV in Fig. 10. In proton therapy, we do not want protons to pass through the tissue, so it is necessary to consider proton energies less than 100 MeV to draw the penetration depth of protons in the breast tissue. These images, where the proton energy values range from 20 to 70 MeV, clearly show the path of the proton particle emitted to the breast tissue. The range of the incident proton is determined so that the location of the maximum proton dose does not exceed the size of the assumed breast (considering a normal breast as a hemisphere, the radius of this hemisphere will be the limit of our assumed breast size; the maximum depth of the assumed breast is shown in Fig. 10 as 50 mm).

The Bragg peak is a fundamental characteristic of proton–matter interactions that plays a pivotal role in radiation therapy. Figure 11 presents a comparative analysis of Bragg peak profiles for two scenarios in the breast tissue irradiated with 60 MeV protons: healthy tissue (breast without a tumour) versus tumour-containing tissue (breast with a tumour).

This comparison elucidates how tumour presence affects the patterns of proton energy deposition and the penetration depth. In this figure,

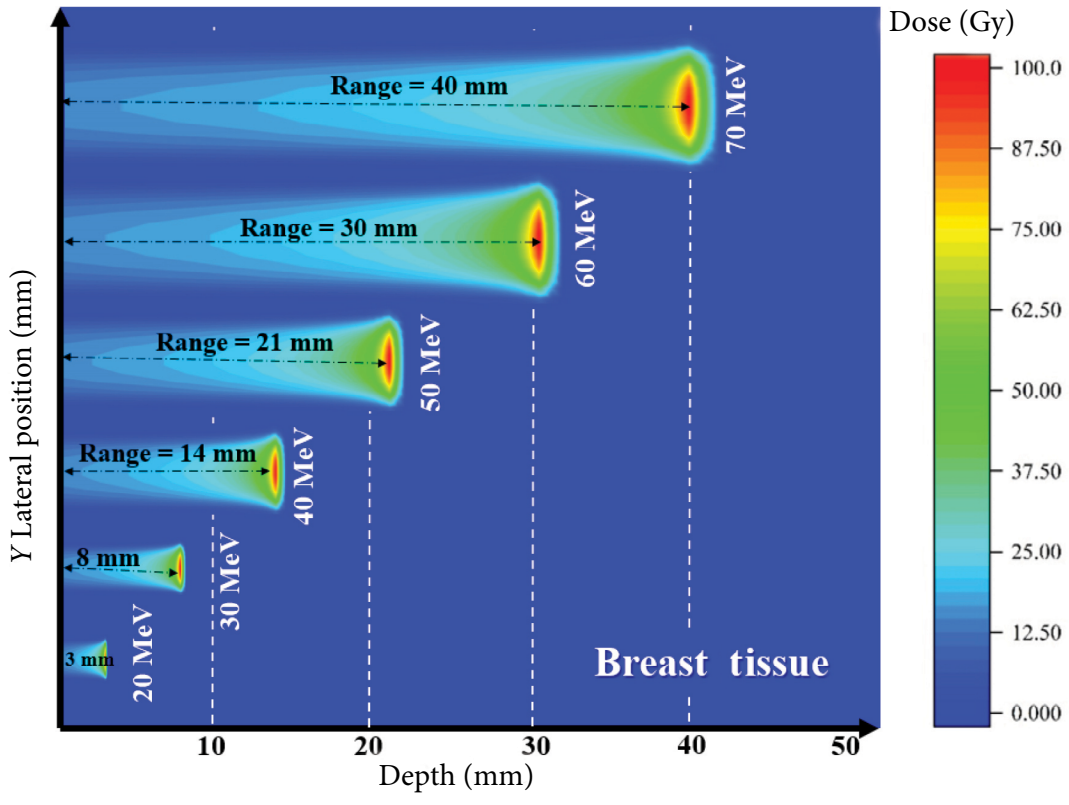

Fig. 10. Diagrams of the 2D dose distribution for a mono-energetic proton pencil beam (with energies of 20, 30, 40, 50, 60 and 70 MeV) in the breast tissue.

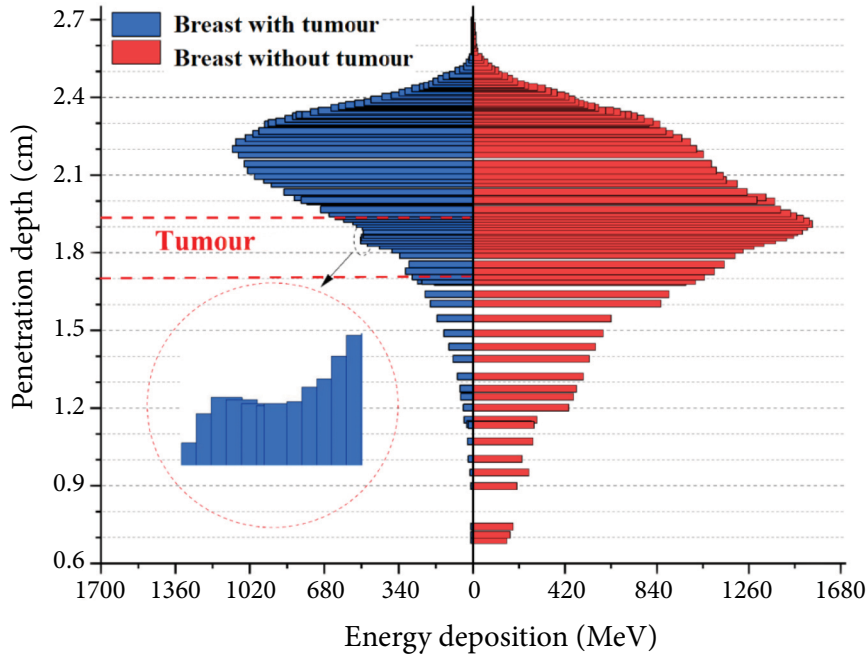

Fig. 11. The Bragg peak for two states without a tumour and with a tumour for the proton energy of 60 MeV in the breast tissue.

the horizontal axis represents the energy deposition (MeV), the vertical axis represents the penetration depth (cm) from the surface of the tumour-free tissue to a certain depth, and a specific Bragg peak is formed in that area. Given that the breast is 5 cm deep, a small tumour is located 1.7 cm deep (a sphere with a radius of 1.2 mm, i.e. from 1.7 to 1.94 cm) from the outer surface of the breast tissue, and the location of tumour tissue is also marked in Fig. 11. The Bragg peak represents the maximum energy absorption by the tumour, and this could be due to the higher density or different chemical composition of the tumour compared to the healthy tissue. On the right, the peak is a result of the broadening of the Bragg peak in the healthy tissue area, the phenomenon of nuclear straggling. In fact, the tumour case shows the formation of a secondary peak. In this figure, a small peak is observed in the tumour area, indicating local energy storage in this area. This secondary peak is formed due to the strong interaction of protons with the tumour material. When the protons reach the tumour, their speed decreases and more energy is deposited in a small volume of the tumour. Also, in the case without a tumour, the proton energy is deposited uniformly at a certain depth, and a clearer Bragg peak is seen. Since all tissues have the same density, we have the broadening of the Bragg peak in the 2 cm volume of the healthy tissue. This decrease may be due to the scattering of the beam or the absorption by healthy tissue. The energy in the healthy tissue is more stable, while in the tumour area there are strong fluctuations. A high tumour density may lead to an increased radiation interaction with matter and a higher energy absorption. However, in the presence of a tumour, the energy distribution changes, and some of the energy is stored in the tumour. This results in a lower peak height and a broader energy distribution. Because the Bragg peak can be focused in a controlled manner on the tumour, proton radiotherapy can minimize damage to the surrounding healthy tissue. This observation helps doctors plan radiation more precisely and ensure that an adequate dose is delivered to the tumour. Therefore, Fig. 11 clearly shows the difference in the energy distribution of protons in the breast tissue with and without a tumour. The presence of a tumour leads to a reduced penetration depth and the creation of a secondary peak in the tumour area. On the other hand, in the Bragg peaks with a tumour and without a tumour with proton energy of 60 MeV, it can be seen that in the case where the tumour is inside the breast tissue, the depth of penetration decreases due to the reduction of some energy

inside the tumour. It can be clearly seen in the magnification that as soon as the beam enters the tumour part, some energy is stored inside the tumour and a small peak is formed. This peak represents the storage of energy inside the tumour and then re-enters the breast tissue and leaves the remaining energy in the breast tissue. These findings not only provide a better understanding of the interaction of protons with different tissues, but are also crucial for optimizing radiation therapy methods. Using this information, more precise and effective treatments can be designed for patients.

Finally, the amount of remaining dose is calculated for two cases with a tumour and without a tumour according to Table 2. To destroy tumours at different depths, it is necessary to have the energy of the incoming protons such that the protons discharge their energy at the tumour site. Considering the location of the hypothetical tumour (from 1.7 to 1.94 cm), it is necessary to consider protons with a certain energy. According to Table 2, in order to destroy the hypothetical tumour, it is necessary to consider the energy of the incoming protons of 60 to 70 MeV to discharge their energy at the tumour site. According to this table, it is natural that when the energy of the incoming protons increases, the range of the protons increases and passes through the tumour site. That is, the energy of the incoming protons is discharged at a location other than the tumour site. In other words, the proton Bragg peak is not formed at the site of our hypothetical tumour. Given that our hypothetical breast depth is 5 cm, protons with energies above 90 MeV will have a range of more than 5 cm, which is outside the depth of the breast. Although in the table, for greater clarity, we have also calculated energies of 100 to 120 MeV.

Table 2. The amount of dose for two conditions without a tumour and with a tumour for breast tissue in terms of energy and depth.

Energy, MeV	Dose, mGy		Depth, cm
	Breast	Breast with tumour	
50	0.736	0.072	0.46
60	0.516	0.051	1.2
70	0.419	0.041	2.06
80	0.383	0.037	3.04
90	0.34	0.033	5.3
100	0.308	0.03	6.6
110	0.285	0.028	7.9
120	0.265	0.026	9.5

4. Summary

Proton radiotherapy is an advanced cancer treatment method that uses high-energy protons to destroy cancer cells with a minimal damage to the healthy tissue. The protons used in this method are mainly produced from deuterium–helium (D–3He) fusion reactions in accelerators. These protons are used in medical imaging (proton radiography) and tumour treatment due to their unique properties, including the Bragg peak. In other words, protons are used in medical imaging due to their ability to pass through different tissues and the dependence of the energy lost on the density of the material. Proton radiography can also show density differences in soft tissues such as the breast with a high accuracy.

Geant4 is a new and powerful Monte Carlo simulation tool that is used in this study to model the interaction of protons with biological tissues and to calculate various quantities and parameters related to protons, secondary neutrons, and gamma photons.

In summary, proton radiotherapy and radiography using protons produced from the D–^{3}He reaction can have a high accuracy in the diagnosis and treatment of breast cancer or other tissues.

The calculations performed with Geant4 show that the presence of a tumour reduces the proton range and changes the dose distribution. In fact, calculating the proton range and stopping power in the breast tissue, penetration depth, and secondary particle flux, and comparing the deposited dose in the breast tissue with and without tumours using Geant4 are among the goals of this study. The results show that the neutron and secondary gamma fluxes should be considered in therapeutic dose calculations to prevent damage to healthy tissues.

Also, comparing the dose in the tissue with and without a tumour confirms that proton therapy can deliver a higher dose to the tumour and spare healthy tissue. These results are useful for optimizing treatment protocols and designing proton imaging systems.

5. Conclusions

In this study, proton radiographs of different human tissues were analyzed by using the excellent capabilities of the Monte Carlo simulation tool of Geant4. Due to the unique properties of proton based on different interaction mechanisms, proton radiography introduces a promising tool in non-destructive tests. These features lead to a better visualization of the internal structure of tissues and even other materials. In this way, we observed that by increasing the proton energy from 50 to 120 MeV, the proton penetrates from 0.46 to 9.5 cm in the breast tissue. According to the location of the tumour, the higher proton energy is able to have its effect on the tumour and destroy the tumour. On the other hand, if the proton energy increases, the quality of the formed image will be better. As seen in Fig. 3, at the proton energy of 118 MeV, the image resolution for the human equivalent tissues, shown in Fig. 2, is best compared to lower energies. Also, according to the obtained results, proton stopping power values for selected tissues increase exponentially and reach the maximum value at about 70 keV with the increase in the energy of radiation protons. In the following, these values begin to decrease exponentially. In fact, this energy is the most suitable energy to destroy cancerous tumours. Further, the depth of proton penetration in the environment of selected tissues increases with the increase of incident proton energy. If the tumour is inside the breast tissue, due to the reduction of some energy inside the tumour, the depth of penetration decreases. Also, in this research, in addition to proton flux, it was tried to focus on neutrons and secondary photons, the amount of dose left in the breast tissue because they help to increase the dose around the tumour area. It can be inferred that the rest of the secondary particles (alpha particles and deuterons) produced deposit most of their energy locally, i.e. close to the production areas, and help to increase the dose delivered to the tumour area without damaging the healthy tissue.

Acknowledgements

We would like to express our appreciation and gratitude for the truly valuable comments of the dear referees, which made the content of the article more coherent and richer.

References

[1] M. Tabak, D. Hinkel, S. Atzeni, E.M. Campbell, and K. Tanaka, Fast ignition overview and background, Fusion Sci. Technol. **26**, 254–276 (2006), https://doi.org/10.13182/FST49-3-254

[2] K.A. Tanaka, R. Kodama, H. Fujita, N. Heya, N. Izumi, Y. Kato, Y. Kitagawa, K. Mima, N. Miyanaga, T. Norimatsu, et al., Studies of ultra-intense laser plasma interactions for fast ignition, Phys. Plasmas. **7**, 2014 (2000), https://doi.org/10.1063/1.874023

[3] V.T. Tikhonchuk, T. Schlegel, C. Regan, M. Temporal, J. Feugeas, P. Nicolaï, and X. Ribeyre, Fast ion ignition with ultra-intense laser pulses, Nucl. Fusion **50**, 045003 (2010), https://iopscience.iop.org/article/10.1088/0029-5515/50/4/045003/meta

[4] M. Tabak, J. Hammer, M.E. Glinsky, W.L. Kruer, S.C. Wilks, J. Woodworth, E.M. Campbell, M.D. Perry, and R.J. Mason, Ignition and high gain with ultrapowerful lasers, Phys. Plasmas **1**(5), 1626–1634 (1994), https://doi.org/10.1063/1.870664

[5] B.F. Towler, *The Future of Energy*, 1st ed. (Academic Press, 2014) p. 157, https://doi.org/10.1016/C2013-0-19049-6

[6] N. Niknam, S.N. Hosseinimotlagh, and Z. Parang, 18FDG production in a PET imaging using a proton flux produced by the D-D fusion reaction, Basic Clin. Cancer Res. **13**(3), 210–224 (2021), https://doi.org/10.18502/bccr.v13i3.11403

[7] S.N. Hosseinimotlagh, N. Niknam, and Z. Parang, Role of GNPS on the enhancement of proton therapy of breast tumor using MCNPX simulation, Res. Sq. (2021), https://doi.org/10.21203/rs.3.rs-955206/v1

[8] S.I. Radwan, S. Abdel Samad, and H. El-Khabeary, Effect of 14.7-MeV protons and 3.6-MeV alpha particles on fusion structural materials, Fusion Sci. Technol. **76**, 710–722 (2020), https://doi.org/10.1080/15361055.2020.1777669

[9] T.Z. Yuan, Z.J. Zhan, and C.N. Qian, New frontiers in proton therapy: applications in cancers, Cancer Commun. **39**, 61 (2019), https://doi.org/10.1186/s40880-019-0407-3

[10] W.D. Newhauser and R. Zhang, The physics of proton therapy, Phys. Med. Biol. **60**, R155–R209 (2015), https://doi.org/10.1088/0031-9155/60/8/R155

[11] H. Paganetti, C. Beltran, S. Both, L. Dong, J. Flanz, K. Furutani, C. Grassberger, D.R. Grosshans, A.-C. Knopf, J.A. Langendijk, et al., Roadmap: proton therapy physics and biology, Phys. Med. Biol. **66**, 05RM01 (2021), https://doi.org/10.1088/1361-6560/abcd16

[12] R.A. Halg and U. Schneider, Neutron dose and its measurement in proton therapy – current State of Knowledge, Br. J. Radiol. **93**, 20190412 (2020), https://doi.org/10.1259/bjr.20190412

[13] C. Domingo, J.I. Lagares, M. Romero-Expósito, B. Sánchez-Nieto, J.J. Nieto-Camero, J.A. Terrón, L. Irazola, A. Dasu, and F. Sánchez-Doblado, Peripheral organ equivalent dose estimation procedure in proton therapy, Front. Oncol. **12**, 882476 (2022), https://doi.org/10.3389/fonc.2022.882476

[14] C.M. Backer, C. Bäumer, M. Gerhardt, S. Ibisi, K. Kröninger, C. Nitsch, J. Weingarten, and B. Timmermann, Evaluation of the activation of brass apertures in proton therapy using gamma-ray spectrometry and Monte Carlo simulations, J. Radiol. Prot. **40**, 848–860 (2020), https://doi.org/10.1088/1361-6498/ab9f42

[15] D. West and A. Sherwood, Proton-scattering radiography, NDT **6**(5), 249–257 (1973), https://doi.org/10.1016/0029-1021(73)90072-8

[16] K. Peach and C. Ekdahl, Particle beam radiography, RAST **6**, 117–142 (2013), https://doi.org/10.1142/S1793626813300065

[17] G. Poludniowski, N.M. Allinson, and P.M. Evans, Proton radiography and tomography with application to proton therapy, Br. J. Radiol. **88**, 20150134 (2015), https://doi.org/10.1259/bjr.20150134

[18] M.C. Levy, D.D. Ryutov, S.C. Wilks, J.S. Ross, C.M. Huntington, F. Fiuza, D.A. Martinez, N.L. Kugland, M.G. Baring, and H.-S. Park, Development of an interpretive simulation tool for the proton radiography technique, Rev. Sci. Instrum. **86**, 033302 (2015), https://doi.org/10.1063/1.4909536

[19] A.J. Mackinnon, P.K. Patel, M. Borghesi, R.C. Clarke, R.R. Freeman, H. Habara, S.P. Hatchett, D. Hey, D.G. Hicks, S. Kar, et al., Proton radiography of a laser-driven implosion, Phys. Rev. Lett. **97**, 045001 (2006), https://doi.org/10.1103/PhysRevLett.97.045001

[20] Y.-C. Tsai, K.-H. Fan, T.-L. Tsai, C.-C. Lee, T. Aso, S.-W. Wu, C.-Y. Lin, C.-K. Tseng, C.-R. Chen, S. Balaji, and T.-C. Chao, Proton radiography using discrete range modulation method – A Monte Carlo study, Radiat. Phys. Chem. **200**, 110279 (2022), https://doi.org/10.1016/j.radphyschem.2022.110279

[21] N.S.P. King, E. Ables, A. Ken, K.R. Alrick, J.F. Amann, S. Balzar, P.D. Barnes Jr, M.L. Crow, S.B. Cushing, J.C. Eddleman, et al., An 800-MeV proton radiography facility for dynamic experiments, Nucl. Instrum. Methods Phys. Res. A **424**, 84–91 (1999), https://doi.org/10.1016/S0168-9002(98)01241-8

[22] C. Arran, C.P. Ridgers, and N.C. Woolsey, Proton radiography in background magnetic fields, Matter Radiat. Extrem. **6**, 046904 (2021), https://doi.org/10.1063/5.0054172

[23] L. Sheng, E. Yuan, F. Yuan, and B. Song, Amide proton transfer-weighted imaging of the abdomen: Current progress and future directions, Magn. Reson. Imaging **107**, 88–99 (2024), https://doi.org/10.1016/j.mri.2024.01.006

[24] L. Chang, X. Xu, G. Wu, L. Cheng, S. Li, W. Lv, D. Pylypenko, W. Dou, D. Yu, Q. Wang, and F. Wang, Predicting preoperative pathologic grades of bladder cancer using intravoxel incoherent motion and amide proton transfer-weighted imaging, Acad. Radiol. **31**(4), 1438–1446 (2024), https://doi.org/10.1016/j.acra.2023.09.044

[25] J. Berthold, C. Khamfongkhruea, J. Petzoldt, J. Thiele, T. Hölscher, P. Wohlfahrt, N. Peters, C. Hofmann, G. Janssens, J. Smeets, and C. Richter, First-in-human validation of CT-based proton range prediction using prompt gamma imaging in prostate cancer treatments, Int. J. Radiat. Oncol. Biol. Phys. **111**(4), 1033–1043 (2021), https://doi.org/10.1016/j.ijrobp.2021.06.036

[26] S. Shiraishi, M. Yamanaka, T. Murai, and K. Tokuuye, Evaluation of delivered doses in proton beam therapy for prostate cancer using positron

emission tomography/computed tomography imaging, Clin. Oncol. **36**(4), 265–270 (2024), https://doi.org/10.1016/j.clon.2024.01.011

[27] Ö.F. Özpolat, B. Alım, E. Şakar, M. Büyükyıldız, and M. Kurudirek, Phy-X/ZeXTRa: A software for robust calculation of effective atomic numbers for photon, electron, proton, alpha particle, and carbon ion interactions, Radiat. Environ. Biophys. **59**, 321–329 (2020), https://doi.org/10.1007/s00411-019-00829-7

[28] P. Sigmund, *Particle Penetration and Radiation Effects*, Springer Series in Solid State Sciences, Vol. 151 (Springer-Verlag Berlin and Heidelberg GmbH & Co. KG, 2006), https://doi.org/10.1007/3-540-31718-X

[29] M. Büyükyıldız, Charged particle interactions of human organs and tissues in heavy ion therapy; effective atomic number and electron density, AKU J. Sci. Eng. **20**(2), 196–206 (2020), https://doi.org/10.35414/akufemubid.692641

[30] M. Büyükyıldız and M. Kurudirek, Radiological properties of healthy, carcinoma and equivalent breast tissues for photon and charged particle interactions, Int. J. Radiat. Biol. **94**(1), 70–78 (2018), https://doi.org/10.1080/09553002.2018.1403057

[31] J. Allison, K. Amako, J. Apostolakis, H. Araujo, P. Arce Dubois, M. Asai, G. Barrand, and R. Capra, Geant4 developments and applications, IEEE Trans. Nucl. Sci. **53**(1), 270–278 (2006), https://doi.org/10.1109/TNS.2006.869826

[32] J. Allison, K. Amako, J. Apostolakis, P. Arce, M. Asai, T. Aso, E. Bagli, and A. Bagulya, Recent developments in GEANT4, Nucl. Instrum. Methods Phys. Res. A **835**, 186–225 (2016), https://doi.org/10.1016/j.nima.2016.06.125

[33] M. Prall, M. Durante, T. Berger, B. Przybyla, C. Graeff, P.M. Lang, C. LaTessa, L. Shestov, P. Simoniello, C. Danly, et al., High-energy proton imaging for biomedical applications, Sci. Rep. **6**, 27651 (2016), https://doi.org/10.1038/srep27651

[34] International Commission on Radiation Units and Measurements, *Tissue Substitutes in Radiation Docimetry and Measurement*, ICRU Report 44 (1989), https://www.icru.org/report/tissue-substitutes-in-radiation-dosimetry-and-measurement-report-44/

[35] K.T. Osman, Stopping powers of protons in biological human body substances (water, tissue, muscles and bones), Int. J. Novel Res. Phys. Chem. Mathematics **7**, 8–12 (2020), https://www.noveltyjournals.com/upload/paper/Stopping%20Powers%20of%20Protons-2236.pdf

[36] K.T. Osman, Mass stopping power and range of alpha particles in adipose tissue, IJSEAS **6**(10), 1–17 (2020), https://doi.org/10.4236/oalib.1110775

[37] A.S. Almutairi and K.T. Osman, Mass stopping power and range of protons in biological human body tissues (ovary, lung and breast), Int. J. Med. Phys. Clin. Eng. Radiat. Oncol. **11**(1), 48–59 (2021), https://doi.org/10.4236/ijmpcero.2022.111005

[38] F.H. Attix, *Introduction to Radiological Physics and Radiation Dosimetry*, Chs. 4, 8 and 10, 1st ed. (John Wiley and Sons, Inc., 1986), https://doi.org/10.1002/9783527617135

[39] M.C. Tufan, and H. Gümüs, Stopping power calculations of compounds by using Thomas–Fermi–Dirac–Weizsäcker density functional, Acta Phys. Polon. A **114**, 703–711 (2008), https://doi.org/10.12693/APhysPolA.114.703

[40] A. Iqbal, N. Ullah, and A.U. Rahman, Density-dependent energy loss of protons in Pb and Be targets and percent mass-stopping power from Bethe-Bloch formula and Bichsel-Sternheimer data within 1–12 MeV energy range: A comparative study based on Bland-Altman analysis, J. Med. Imaging Radiat. Sci. (JMIRS) **50**, 149–156 (2019), https://doi.org/10.1016/j.jmir.2018.10.003

[41] W. Bragg and R.B.Sc. Kleeman, On the α particles of radium and their loss of range in passing through various atoms and moleculs, Lond. Edinb. Dubl. Phil. Mag. **10**, 318–340 (2009), https://doi.org/10.1080/14786440509463378

SIMULIUOTOS ŽMOGAUS AUDINIO TERPĖS RADIOGRAFIJA IR RADIOTERAPIJA NAUDOJANT AUKŠTOS ENERGIJOS PROTONUS: TEORINIS TYRIMAS

N. Niknam [a], M. Eshghi [b], S.N. Hosseini Motlagh [a], Z. Parang [a]

[a] *Islamiškojo Azado universiteto Fizikos fakultetas, Širazas, Iranas*

[b] *Imamo Hoseino universiteto Fizikos fakultetas, Teheranas, Iranas*